NASA DEVELOP National Program
Idaho – Pocatello

Summer 2022

Idaho Wildfires

Assessing Drought and Fire Conditions, Trends, and Susceptibility to Inform State Mitigation Efforts and Bolster Monitoring Protocol in North-Central Idaho

DEVELOP Technical Report

Final – August 11, 2022

Ford Freyberg (Project Lead)
Brenner Burkholder
Jessica Hiatt
Carson Schuetze

Advisor:
Keith Weber, Idaho State University, GIS Training and Research Center (Science Advisor)

Fellow:
Brandy Nisbet-Wilcox (Idaho Fellow)

1. Abstract

Escalating severity and frequency of drought and wildfire call for effective and cost-efficient mitigation planning and monitoring protocols. The Palouse ecoregion, an agricultural epicenter in North-central Idaho, is of particular concern as both drought and wildfire present substantial economic threats. The DEVELOP team implemented Earth observation data to assist the Idaho Office of Emergency Management, Idaho Department of Water Resources, and Idaho Department of Lands in updating the state's Hazard Mitigation Plan by enhancing their drought and fire monitoring capabilities. The team utilized Landsat 8 Operational Land Imager (OLI), and Aqua and Terra's Moderate Resolution Imaging Spectroradiometer (MODIS), along with ancillary datasets, to assess drought indicators and map hazard susceptibility. The team upgraded the state's current fire hazard model by updating existing data layers and adding drought indicator data to support partners' continued assessment of fire hazard conditions. The team observed Evaporative Demand Drought Index (EDDI) spikes during the highest fire occurrence and burned area years in the study period: 2015 and 2021. Models from dry, high fire occurrence and burned area year 2015 outperformed models from mesic, low fire occurrence and burned area year 2016. The increased understanding of drought conditions and fire susceptibility in this ecosystem will assist partners in improving land management practices.

Key Terms: wildfire, drought, Landsat, NDVI, EDDI, ESI, fire hazard, hazard modeling

2. Introduction

2.1 Background Information

The area and frequency of wildfires in the Western United States have grown over recent decades. From 1984 to 2011, the total area burned and number of large wildfire incidents (>1,000 acres) increased annually by 355 square kilometers and 7 incidents, respectively (Dennison et al., 2014). Additionally, "mega-fires" greater than 100,000 acres have increased in frequency from 1950 to 2019 (Weber & Yadav, 2020). See Figures A1-A5 in Appendix A for Idaho- and study area-specific fire trend data.

While some regions have exhibited lower drought severity in recent years, the Southwest and West have endured increased hydrological and soil moisture drought severity and corresponding vegetation stress (Apurv & Cai, 2021). This is a continuation of the multidecadal drought pattern in the Southwest and West, which experienced increased drought duration and severity from 1925 to 2003 (Andreadis & Lettenmaier, 2006). In Idaho, heightened growing season maximum temperatures were expected to elevate evapotranspiration (ET), driving additional drought pressure in the state if combined with lower precipitation levels (Sohrabi et al., 2013). However, a pilot study of the Intermountain West region found that while climate variables drive vegetation production to a significant extent, no significant changes to precipitation or maximum temperature were observed from 2000–2020 (Yadav et al., 2020).

Drought and wildfire alike generate risk for natural and built environments and their inhabitants. Susceptibility to these phenomena involves a complex, overlapping mix of variables and conditions. For example, drought stress can increase fuel load from dead plants, leading to larger, more intense fires (Li et al., 2020). Similarly, live vegetation biomass, primarily affected by the seasonal moisture cycle, can desiccate due to unseasonably hot and dry conditions. When preceded by high volumes of spring vegetation growth, drought conditions elevate the risk of fire.

In a review of drought and wildfire across the Western U.S. over the last 750 years, fire was more prevalent in characteristically cooler, wetter regions during warm, dry periods (Scasta et al., 2016). Opposite effects were observed in arid regions, where drought conditions may reduce fire occurrence (likely due to reductions in biomass). These studies highlight regional specificities in the drought-fire relationship and emphasize that fire susceptibility increases when drought conditions follow heavy growth, while susceptibility is lower in the opposite circumstance.

2.2 Study Area & Period

The team analyzed drought and wildfire trends in North-central Idaho, defining a study area that included the Palouse Prairie ecoregion as well as surrounding forest, shrub, and grassland, across a range of elevations. This diversity of ecoregions and land features improves reproducibility for future study regions. Furthermore, the study area falls completely within a corresponding Landsat 8 OLI path, enabling same-day image composites across its entirety. The study period was 2013–2021.

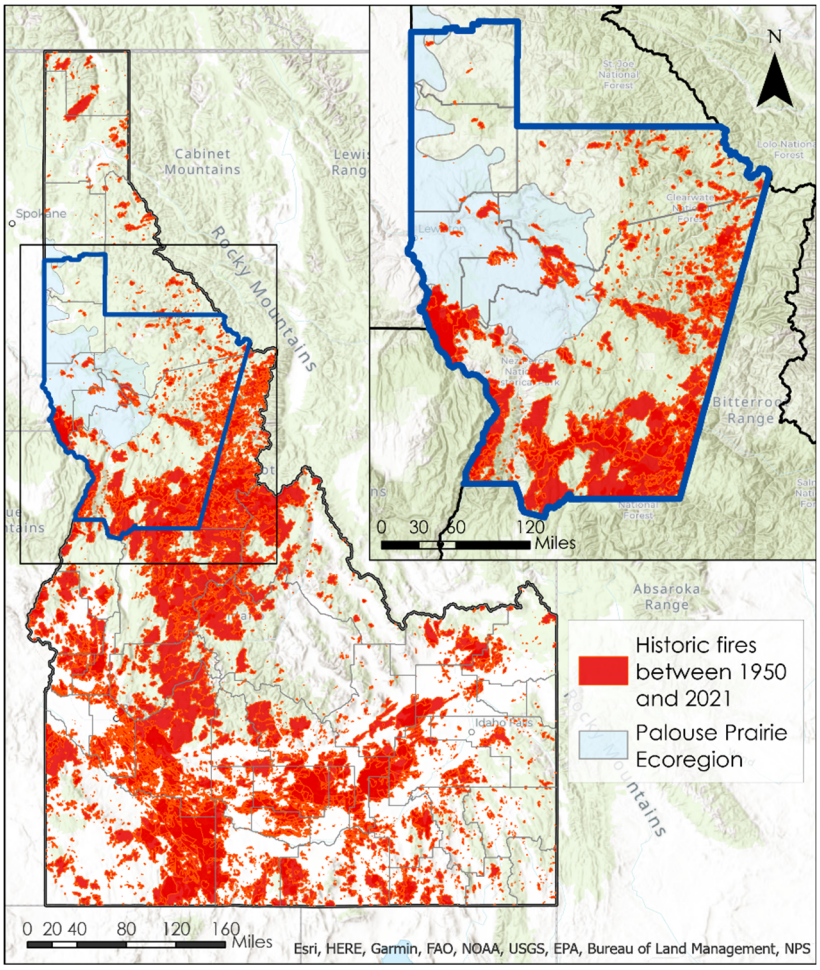

Figure 1. The state of Idaho with historical fires 1950–2021 demarcated in red; the current study region outlined in dark blue and highlighted in the inset. Light blue shading indicates the Palouse Prairie ecoregion.

2.3 Project Partners & Objectives

The team partnered with the Idaho Office of Emergency Management (IOEM), Idaho Department of Water Resources (IDWR), and Idaho Department of Lands (IDL), who coordinate hazard mitigation plans for the state of Idaho. These include the Idaho Drought Plan (2001), the Idaho State Hazard Mitigation Plan (2018), and the Idaho Statewide Implementation Strategy for the National Fire Plan (2006). Existing wildfire mitigation efforts focus on creating fire-resistant landscapes and fire-adapted communities, reducing ignition and fuel sources, rehabilitating grassland and forested areas, and increasing public awareness. Existing drought mitigation efforts focus on weather modification, improving water quality, reducing water waste, and restoring damaged ecosystems.

Understanding the condition and trends of both drought and wildfire is essential for partners to continue their work. Therefore, the team aimed to trace the history of fire and determine trends in two drought indicators: Evaporative Demand Drought Index (EDDI) and Evaporative Stress Index (ESI). Using those assessments, the team recreated IDL's static wildfire hazard model and updated it with the most recent data.

The team then generated hazard models enhanced with dynamic drought and fuel-proxy data for each year in the study period and analyzed outputs for accuracy. Finally, the team created a step-by-step protocol for partners to build the optimized model. These products were intended to assist partners in updating their state hazard mitigation plans, contextualize drought and wildfire in the study area, and help inform drought and wildfire resource staging.

3. Methodology

3.1 Data Acquisition

EDDI and ESI are indices used to assess drought conditions and potential. These indices are created across composite timeframes ranging from daily to several months. The team acquired EDDI 4-week Daily CONUS 13km data product from the National Oceanic and Atmospheric Administration (NOAA) Physical Sciences Laboratory (PSL) for the study period. The team also retrieved ESI 4-week Daily Global 5km data as geotiffs from the NASA SERVIR ClimateSERV Application. See equations B3 and B4 for respective EDDI and ESI calculation.

The team acquired Dynamic World data (AI-produced highest probability near real-time land cover data) for the months of March–September, for the entire study period. Data from Keith Weber at ISU, included NASA RECOVER products for elevation, degree of slope, and aspect which provided continuous topographic data for the study area. In addition, the Historic Fires Database (HFD) was downloaded and provided historical fire perimeters from 1950 to 2021 (Weber 2022). The team also acquired Federal Emergency Management Agency (FEMA) Wildland Urban Interface (WUI) data from partners at IDL. Acquisition of these data products is summarized in Table 1.

Landsat 8 OLI scenes in path 42 rows 27 and 28 with less than 30% cloud cover were acquired for growing and fire seasons in study period years, first using the Earth Explorer website through USGS and later with USGS/EROS Machine-to-Machine API. Because the study area fell entirely within one Landsat path, same-day scenes covering the study area were considered statistically comparable. The team only acquired Landsat scenes for which both path/row 042/027 and 042/028 met criteria. Afterwards, the team clipped Terra MODIS 16-day 250m data, provided by Keith Weber, to the Western United States in the USA Contiguous Albers Equal Area Conic (WKID 102039) coordinate system. See Table 2 for summary of these NASA data products.

Table 1
List of datasets utilized for this project

Source	Data Product	Dates	Acquisition Method
NOAA – PSL	Evaporative Demand Drought Index (EDDI): 4-week Daily CONUS 13km	2013–2021	Scripted download from NOAA data archive
Keith Weber, GIS Training and Research Center at Idaho State University and USGS	NASA RECOVER value added National Elevation Dataset	2016	From Keith Weber, ISU
Google, World Resources Institute	Dynamic World 10m V1 – Based on ESA Copernicus Sentinel-2 MSI Level 1C data	Mar. 1 – Sep. 30, 2021	Google Earth Engine script and TIF download

Keith Weber, Idaho State University GIS Training and Research Center	Historical Fires Database	1950–2021	From Keith Weber, ISU
FEMA Hazard Mitigation Plan	Wildland Urban Interface (WUI)	2022	From Tyre Holfeltz, IDL
NASA MSFC/SPoRT	Evaporative Stress Index (ESI): 4-week Daily Global 5km	2013–2021	SERVIR ClimateSERV Application
LANDFIRE, Earth Resources Observation and Science Center	LANDFIRE Existing Vegetation Type	2020	From Keith Weber, ISU
USGS and USDA	National Watershed Boundary Dataset 12-digit hydrologic unit (HU)	2022	ArcGIS Portal

Table 2
List of NASA sensors and data products utilized for this project

Platform and Sensor	Data Product	Dates	Acquisition Method
Landsat 8 OLI	Landsat 8 Operational Land Imager and Thermal Infrared Sensor Collection 2 Level-1	Mar. 1–Sep. 30, 2013–2021	Earth Explorer download & USUS/ EROS Machine-to-Machine API
Aqua/Terra MODIS	MOD13Q1 v006-MODIS/Terra Vegetation Indices 16-Day L3 Global 250m SIN Grid	Feb. 28–Oct. 3, 2013–2021	From Keith Weber, ISU

3.2 Data Processing

After acquiring Landsat 8 OLI scenes, the team used TerrSet to import and atmospherically correct the Collection 2 Level-1 data into reflectance data using the cosine approximation model (COST). The TerrSet VegIndex module provided Normalized Difference Vegetation Index (NDVI) while the ImageCalculator module provided Normalized Difference Moisture Index (NDMI) rasters for each combination of same-day Landsat 8 OLI scenes (Equations B1 & B2). Following this, the team shifted processing to ArcGIS Pro to remove clouds from corrected NDMI and NDVI rasters. The QA-PIXEL band served as a mask to remove pixels with quality assurance issues (e.g., cloud contamination) from further processing. Each NDVI and NDMI date-specific imagery pair was then mosaiced to create a single, cloud-free raster image by date using Python scripts for the ArcGIS Pro 'Times' and 'Mosaic' geoprocessing tools. Mosaics were then batch-projected to WKID 102039 and clipped to the study area.

Regular time intervals were required to conduct a time series analysis using NDVI, but heavy spring cloud cover prevented the team from using Landsat's 16-day return interval imagery. The team created composite Landsat/MODIS NDVI images for the missing dates. The team resampled MODIS NDVI to 30m to match Landsat's resolution. Due to time constraints, composites were only created for 2015 and 2016. All MODIS and Landsat images within 32 days of the missing dates were included in calculations for the composite images. The team used a weighted average so that images nearest the missing date had the greatest influence on the composite image. For example, the team created a composite image for 8/14/2015 using images from 8/12/2015 (MODIS) at a weight of 16/18 and from 7/29/2015 (Landsat) at a weight of 2/18.

The team generated a highest probability landcover raster for all of Idaho for Mar. 1–Sep. 30, 2021 in Google Earth Engine (GEE) using the Dynamic World 10m V1 dataset. This classified product was clipped to the study area in GEE before being exported as a GeoTIFF in EPSG 5070 (NAD83/Conus Albers) and

imported to ArcGIS Pro. EDDI data was in ASCII format with an unknown spatial reference system presumed to be WGS 1984 and therefore the team defined it as such and reprojected it into WKID 102039. Then the team reprojected the ESI data (GeoTIFFs format) to WKID 102039. Both EDDI and ESI raster datasets were then batch-clipped in ArcGIS Pro.

Next, using ArcGIS Pro's Raster to Point tool, the team generated centroid points of EDDI pixels as extraction points for drought indicator data throughout the analysis phase. EDDI was the dataset with the coarsest spatial resolution (13km), therefore, the team based the extraction points on EDDI's pixel size to avoid oversampling the same EDDI pixel during analysis. This process generated 165 features for extraction. The team sampled the weekly EDDI and ESI rasters at these points for each year in the study period, before exporting these tables as CSV files for trend and time-series analysis in Microsoft Excel and R Studio. The team also extracted Dynamic World information to distinguish landcover classes.

For the wildfire hazard modeling phase of the analysis, the team sliced the HFD by year for each year in the study period, creating a fire frequency layer for each year in the study period (e.g., the 2019 fire frequency layer contained all fires from 1950-2019 while the 2020 fire frequency layer contained all fires form 1950-2020). Then, the team calculated burn density within each subwatershed by dividing the sum of historical acres burned by the subwatershed area. These yearly feature layers were then rasterized at 30 m pixels for use in the model. WUI and topography data were projected to WKID 102039 and clipped. Based on IDL's specified categorization scheme, the team classified each vegetation type in the LANDFIRE dataset as one of 6 categories: grass-tree, grass-shrub, shrub, shrub-tree (including pinyon and juniper), and tree.

Using ArcGIS Pro's Resample tool with bilinear resampling, the team resampled EDDI and ESI weekly rasters to 30 m resolution to match other model datasets. Bilinear interpolation calculated the resampled value for each pixel based on the distance-weighted average of the surrounding 4 pixels. The Cell Statistics tool in ArcGIS Pro allowed the team to then extract median fire season (6/1–9/30) EDDI and ESI in the study area for each year in the study period. The team also used Cell Statistics to generate median growing (3/1–6/1) and fire season NDVI from the composite Landsat/MODIS NDVI dataset. With these median NDVI rasters from each season, using the Raster Calculator, the team generated an NDVI-difference raster by subtracting the median fire season NDVI from the median growing season NDVI.

All wildfire hazard model datasets required reclassification to meet the model's categorization paradigm. The team reclassified historic fires, slope degrees, aspect, WUI, and vegetation class according to the values and ranges in Table 3. The team based the reclassification on IDL's existing wildfire hazard model scheme.

Table 3
Reclassification scheme for wildfire hazard model variables.

Variable	0	1	2	3	4	5	6
Slope (degrees)	-	0–10	10–20	> 20	-	-	-
Aspect (degrees)	Flat	N (0–45, 315–360)	E (45–135)	S, W (135–315)	-	-	-
Burn density (acres/acre)	0	0–0.5	0.5–1.0	> 1.0	-	-	-
WUI	-	Is not WUI	-	Is WUI	-	-	-
Vegetation Class	-	Grass	Grass-Tree	Grass-Shrub	Shrub	Shrub -Tree	Tree

Column headers indicate values used in the model based on the given continuous or categorical range. N refers to aspect North, E to aspect East, S to aspect South, and W to aspect West.

The reclassification values for EDDI, ESI, and NDVI difference are shown in table 4. The team based the drought reclassification values on the US Drought Monitor's Drought Classification percentile scheme: 2nd,

5th, 10th, 20th, 30th, 70th, 80th, 90th, 95th, and 98th percentiles. The percentiles correspond to established categories: Exceptional Wetness (EW4), Extreme Wetness (EW3), Severe Wetness (EW2), Moderate Wetness (EW1), Abnormally Wet (EW0), Abnormally Dry (ED0), Moderate Drought (ED1), Severe Drought (ED2), Extreme Drought (ED3), and Exceptional Drought (ED4), respectively.

Table 4
Reclassification scheme for wildfire hazard model variables.

Variable	-4	-3	-2	-1	0	1	2	3	4
EDDI	≤ -2.054	-2.054– -1.926	-1.926– -1.712	-1.712– -1.284	-1.284– 1.284	1.284– 1.712	1.712– 1.926	1.926– 2.054	≥ 2.054
ESI	3.5– 3.36	3.36– 3.15	3.15– 2.8	2.8– 2.1	2.1– -2.1	-2.1– -2.8	-2.8– -3.15	-3.15– -3.36	-3.36– -3.5
NDVI-difference	-1.4– -1.25	-1.245 -1.1	-1.1– -0.8	-0.8– -0.2	-0.20– 0.4	0.4– 1	1.0– 1.3	1.30– 1.45	1.45– 1.60

Column headers indicate values used in the model based on the given continuous range.

3.3 Data Analysis

3.3.1 Drought Indicator Analysis

The team assessed EDDI and ESI via time series analysis stratified by landcover. The team also compiled MODIS NDVI into a time series. The full time series as well as individual years were investigated. The team experimented with a variety of lag periods, moving average, and visualization options to best explore and display trends in drought data over the study period. The team used Microsoft Excel for initial data organization and visualization. In addition, R Studio (packages including: forecast, ggplot2, tidyverse, and lubridate) offered robust data manipulation, analysis, and visualization capabilities. The team explored various statistical analysis methods to determine if EDDI or ESI showed any forcing influence on NDVI. See Figure C1 in Appendix C for a flowchart of Drought Indicator Analysis.

3.3.2 Wildfire Hazard Modeling

Upon reclassifying continuous data into categorical fire hazard-weighted values, the team generated wildfire hazard models for each year in the study period. For each year the model incorporated: historical burn density, WUI data, slope degrees, aspect, median fire season EDDI or ESI (only one drought indicator was used in any given model due to high intercorrelation), and vegetation class. Select model years included spring-summer NDVI difference. The sum of the reclassified weights, generated with ArcGIS Pro's Raster Calculator tool, served as the overall wildfire hazard score for a given pixel. The categorization of hazard levels was based on IDL's technique of finding Jenk's natural breaks in the data. Further optimization by the team allowed for comparison across years, maps, and models: percentile breaks determined cutoffs for ascending hazard levels. Type I and Type II models both served as prototypes for potential categorical breakpoint paradigms. The team calculated a pixel's 'percentile' by taking its hazard model actual score divided by the maximum possible hazard score for that model. This way, categorical breaks were decided not based on the raw hazard score (which changed frequently between models), but the percentage of the maximum hazard score, allowing for easier comparisons. Type I models utilized the following percentile breaks for hazard score: 0–27%, 27–46%, 46–64%, 64–77%, and 77–100%. Type II models used these values: 0–27%, 27–46%, 46–55%, 55–77%, and 77–100%.

Ultimately, the team generated many model iterations for every year in the study period. Type I and Type II models offered alternative breakpoints for the following models in each year: base model, consisting only of IDL's variables (updated with corrected and/or more recent data); ESI-enhanced; EDDI-enhanced; and spring-summer NDVI difference-enhanced. One limitation or problem encountered early in the study was related to the WUI data. These data suffered from limitations, including inconsistent WUI definitions between counties and indications of WUI using simple point features as opposed to rasters or polygons.

The team assessed accuracy in a variety of exploratory ways. One method for accuracy assessment involved calculating the number of true burn pixels in the model year that fell within the highest two hazard categories (Moderate-High and High). This "True-Positive" percentage gave an indication of how many of the highest risk pixels actually burned in a given year. The team defined "False-Positives" as Moderate-High and High fire hazard pixels that did not actually burn in the given year; "True-Negatives" as Low, Moderate-Low, and Moderate fire hazard pixels that did not burn; and "False-Negatives" as Low, Moderate-Low, and Moderate fire hazard pixels that did burn. As the team cycled through iterations of models, maximizing "True-Positives" while attempting to limit "False-Positives" served as a guiding principle. The team developed another experimental accuracy assessment protocol in consultation with partners that assessed only true burn pixels. For true burn pixels, the team extracted the pixel's classified hazard category from the model to determine the distribution of categories. Models exhibiting higher percentages of high-hazard true burn pixels were considered to have outperformed those with lower percentages of high-hazard true burn pixels. See Figure C2 for a flowchart of Wildfire Hazard Modeling analysis.

4. Results & Discussion

4.1 Analysis of Results

4.1.1 Drought Indicator Analysis

Time series data on drought indicators showed spikes in the 8-week moving average of EDDI preceding the fire seasons with largest area burned, 2015 and 2021(Figure 2). EDDI values above 1.28 cross the threshold into the official drought category for moderate drought, EDDI values above 1.71 cross the threshold into severe drought, and values above 1.93 cross the threshold into extreme drought. All values above 0 indicate anomalous evaporative demand.

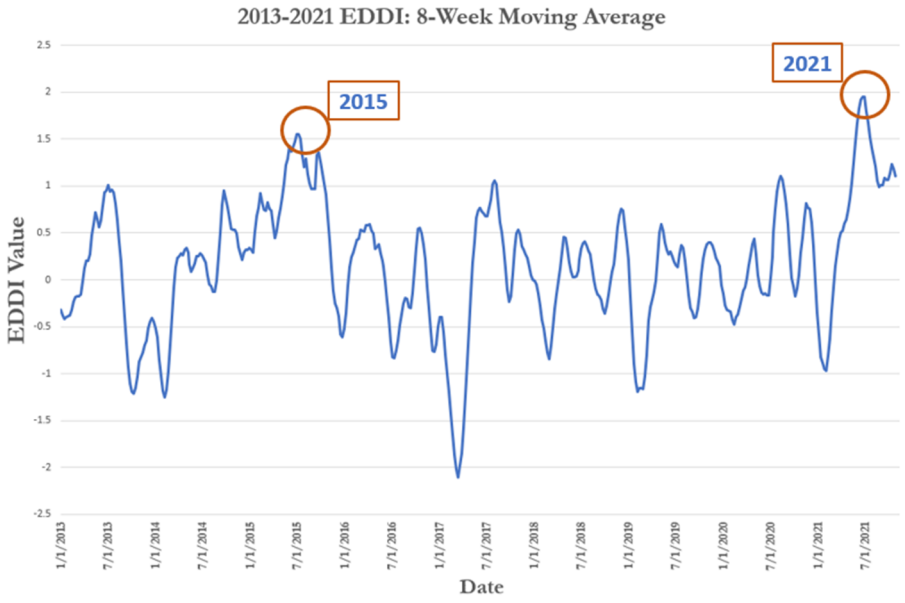

Figure 2: Eight week moving average of 4-week median EDDI data for the study area in forested landcover. Years with the largest area burned (2015, 2021*)* are highlighted with orange.

By this metric, median EDDI across all pixels in the study area fell into the moderate drought category in 2015, though it did approach severe drought. In 2021, median EDDI fell squarely in extreme drought and approached exceptional. These values represented the median across all pixels in the study area; specific regions of the study area did maintain other drought categorizations throughout portions of 2015 and 2021 fire seasons.

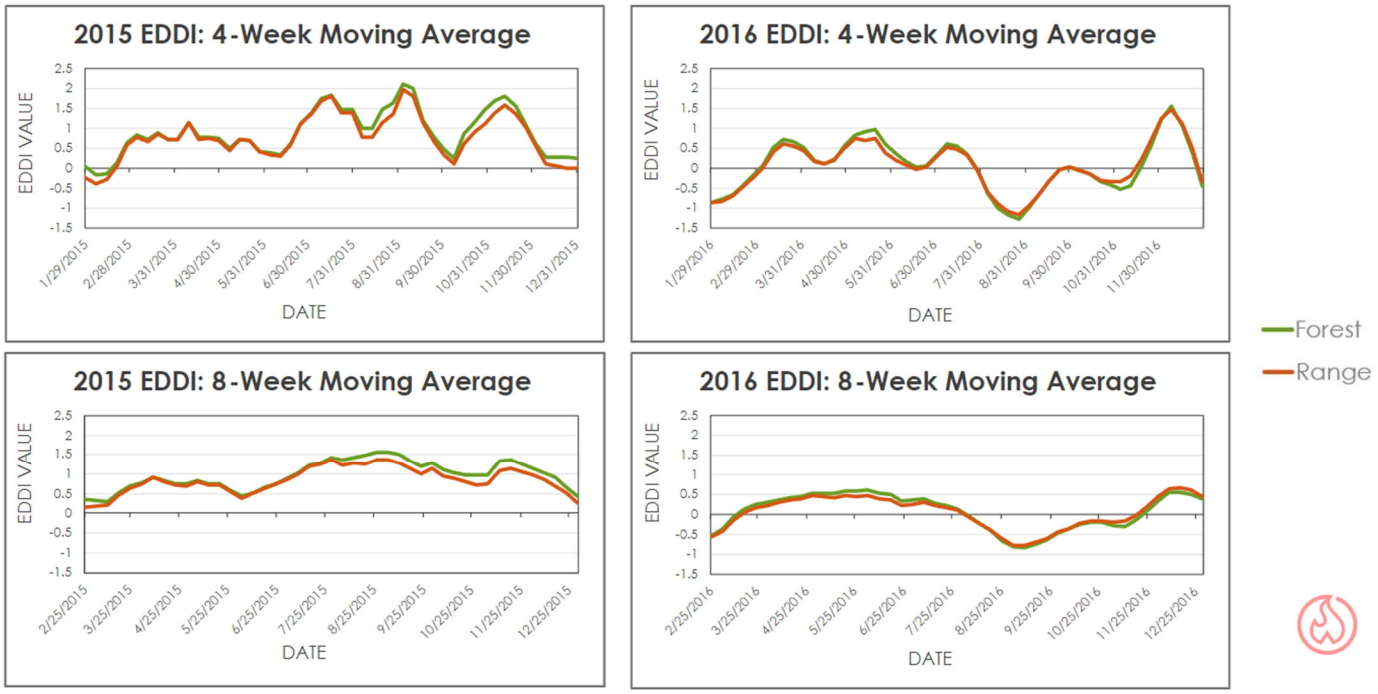

Figure 3: 4- and 8-week moving average of 4-week median EDDI in study area across study period in forested (green) and rangeland (orange) landcover for 2015 and 2016.

Looking specifically at case-study years of 2015 (dry, high fire frequency and area burned year) and 2016 (mesic, low fire frequency year) gave indication of the EDDI dynamics within individual years (Figure 3). The 2015's drought stress becomes apparent when considering its consistent moving average values above 0, and often reaching the maximum value of 2. Meanwhile, in 2016 both 4- and 8-week moving averages displayed a tendency to hover around 0 and even dip below that median threshold, especially in peak fire season. Overlaying NDVI and EDDI time series data for the entire study period showed interactions between these variables (Figure D1, Appendix D). Autocorrelation analysis of each of these time series (Figure D2, Appendix D) indicated that NDVI was highly autocorrelated (indicating periodicity) while EDDI did not show signs of autocorrelation. The team attempted basic cross-correlation analysis (Figure D3, Appendix D), hoping to discover a correlation at specific lag periods. Significant correlations did exist but periodicity and autocorrelation of NDVI prohibited clear conclusions from being drawn.

NDVI difference in case study years 2015 and 2016 highlighted the potential utility of this fuel load and dryness proxy (Figure 4). Comparing the histograms of these raster layers showed that in years without significant drought (e.g., 2016), NDVI difference largely remained clustered around 0. This indicates minimal changes to NDVI between growing and fire season for the vast majority of pixels. In contrast, 2015 showed a similar peak but a positive skew with many values exhibiting large NDVI declines between seasons. The team interpreted this as evidence supporting the idea that in drought pressure years NDVI loss — and consequent drying of fuels — is greater than in temperate years. One factor that may have affected these NDVI difference values could be NDVI loss from fires. If a fire occurred early enough in the year, or if cloud cover reduced the number of available NDVI rasters throughout fire season, the median value might pick up the severe drop off in NDVI following actual fire. Based on the team's exploration of several fires in 2015, evidence for this possible source of error was not apparent. Additionally, though 2015 was a big fire year, only 4.21% of the study area burned, a total insufficient to account for the disparity seen in the histograms.

a.

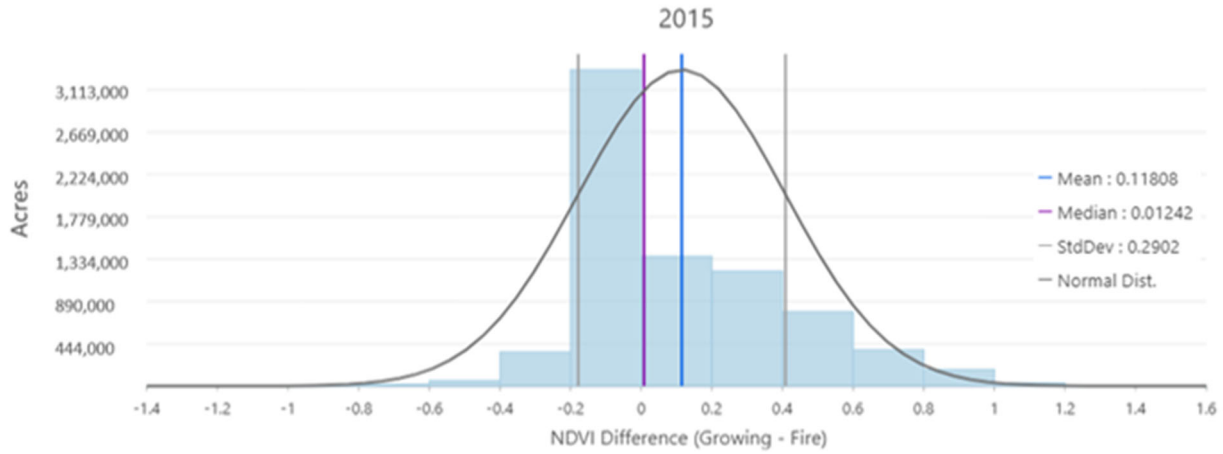

b.

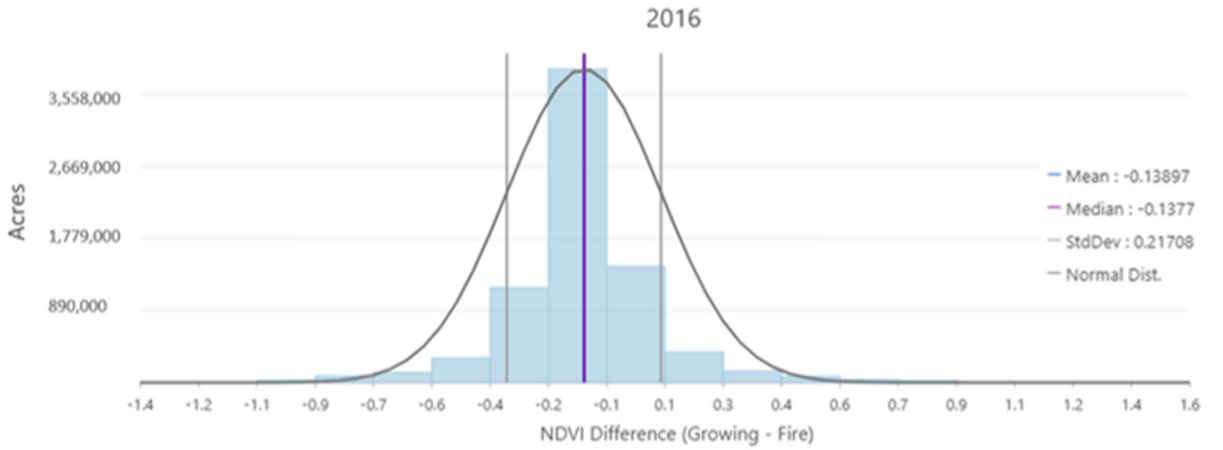

Figure 4: Histograms for NDVI difference (growing season NDVI – fire season NDVI) rasters of the study area from 2015 and 2016, including all landcover types. One standard deviation denoted with grey vertical bars, median denoted with purple vertical bar, mean indicated with blue vertical bar. Normal distribution indicated with dark grey curve.

4.1.2 Wildfire Hazard Modeling

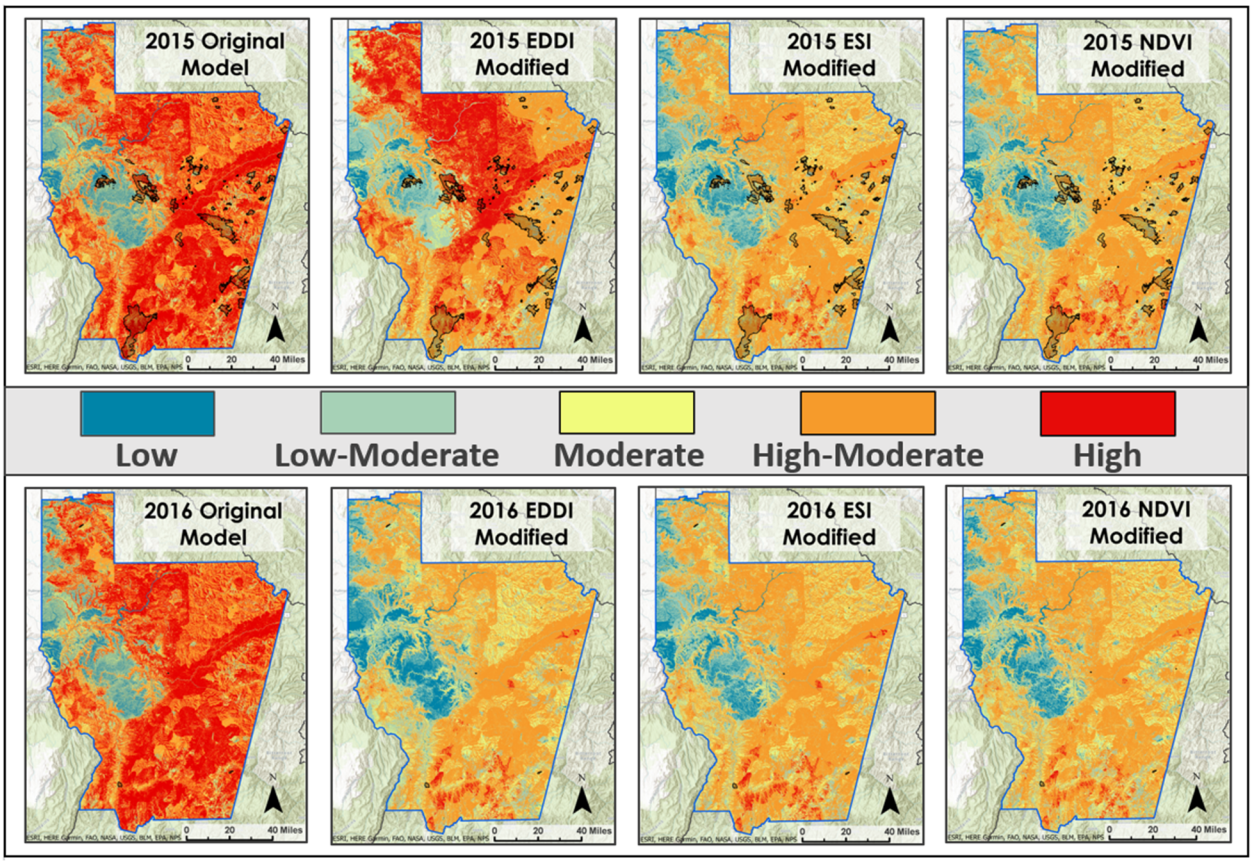

Figure 5: Original, EDDI, ESI, and NDVI-difference fire hazard models for 2015 (top) and 2016 (bottom). Black polygons represent fires from that year (2016 had very few and very small fires - notice small black dots in lower left and lower right of study area).

The team completed many iterations of the wildfire hazard model, searching for visual differences and testing accuracy using aforementioned methods. The years 2015 and 2016 proved valuable case study years, as 2015 was dry and fire prone, while 2016 was temperate and suffered few fires. Therefore, the team selected these years to display model results. Figure 5 shows a panel of model outputs highlighting the original, EDDI-enhanced, ESI-enhanced, and NDVI difference-enhanced models. The team noticed a similarity between base models in the two case study years, indicating insufficient dynamic wildfire hazard prediction capability. For drought-enhanced models, the difference between the case study years often proved apparent, potentially capturing real differences in wildfire hazard between years. The team found that model performance in a dry year (2015) exceeded the performance in a wet year (2016), when performance is characterized in terms of greatest proportion of true positive pixels, though these models at times suffered from outsized percentages of false positives. The EDDI model and the original model performed better than the NDVI and ESI model for 2015 in terms of true positives, though the NDVI and ESI models exhibited much higher true negative percentages.

This indicated that while the original and EDDI models are capturing more true burn pixels, this may have been due to general over-prediction of high hazard areas. The original models for 2015 and 2016 scored the two highest False Positive percentages of all models tested. In 2016, the NDVI model performed best in True Negative percentage by over 4%, while all models showed True Positive percentages that rounded to zero. Fire susceptibility and occurrence accuracy proved tricky; "low susceptibility" areas may burn because ignition sources were present, while areas at very high risk might be spared due to lack of ignition. A visualization of the alternative, burn-area only accuracy assessment can be found in Figure 6. This method of measuring accuracy does not take false positives, or over-prediction, into account.

Table 5
Accuracy statistics for models in Figure 5.

Model	True Positive %	True Negative %	False Positive %	False Negative %
2015 Original	3.7%	23.8%	72.0%	0.5%
2015 EDDI	3.5%	25.5%	70.2%	0.7%
2015 ESI	2.9%	40.5%	55.3%	1.4%
2015 NDVI	3.0%	41.3%	54.7%	1.3%
2016 Original	0.0%	23.8%	76.2%	0.0%
2016 EDDI	0.0%	42.2%	57.8%	0.0%
2016 ESI	0.0%	42.2%	57.8%	0.0%
2016 NDVI	0.0%	46.7%	53.2%	0.0%

True Positive% and False Negative% for 2016 models rounded to 0.0% at one decimal place.

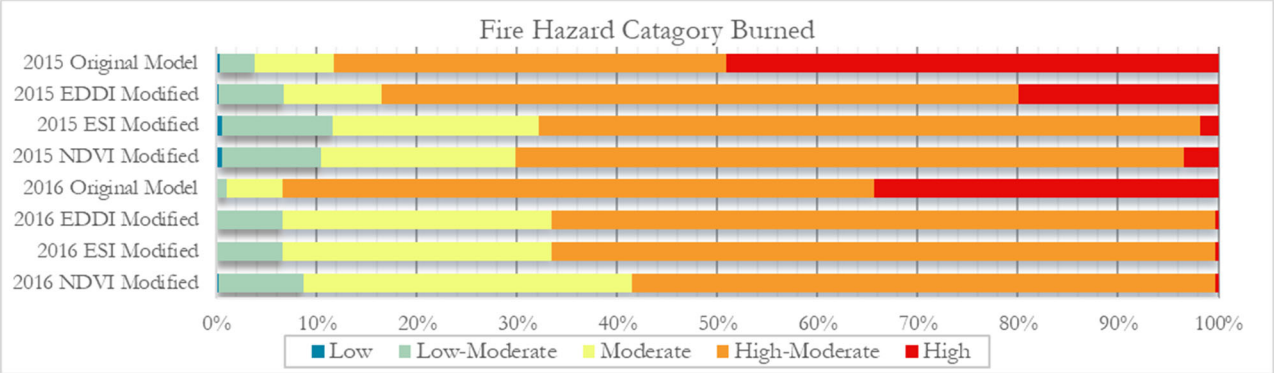

Figure 6: Category distribution of burned acres from models in 2015 and 2016.

4.2 Future Work

The primary future direction identified by the Idaho Wildfires Term I team revolves around wildfire hazard model improvement. The existing base model, along with all enhanced iterations, could serve as a useful launch point for models offering better prediction of fire hazard areas with less of a propensity for overprediction. In addition to improved accuracy, a critical feature of the optimized model must be the capacity to run the model in near real time using the most recent available drought and NDVI data. EDDI and ESI are available within five days while Landsat imagery is often available within hours of acquisition. This would greatly enhance the model's usefulness and practicality.

The team recognized dynamic WUI, landcover, and vegetation class data as a key area for possible improvement of the model. As it stands, the best available WUI data (not obtained until week nine of the initial ten-week term) were based on the 2020 Census but were applied back to the 2013 model. For landcover and vegetation class, especially in the context of vegetation incineration and landscape degradation in the aftermath of wildfire, using static data across all years of the model may have limited these variables' effectiveness at differentiating hazard levels between years. Dynamic World and LANDFIRE data products are available across different years, and incorporating a dynamic approach to these variables could improve model accuracy. In addition, the breakpoint thresholds for fire hazard categories in the model were somewhat arbitrary. The team attempted to set reasonable breakpoints based on IDL's existing Jenk's natural breaks scheme and tweaked the scheme to utilize percentages rather than raw values for comparison purposes, but further optimization of breakpoints could improve model performance.

The team saw significant gaps in model performance in wet/low fire years and dry/high fire years. This was not inconsistent with established wildfire modeling literature, where it is common to find multiple versions of models: one for wet years and one for dry years (Chuvieco et al., 2010). Upon consultation with partners, the

team gained a crucial insight, though too late in the term to capitalize on it: because of biophysical differences in vegetation response to drought between forests and rangeland, these landcover classes ought to be differentiated for drought indicator application. Rangeland, dominated by grasses and shrubs, could see fuel drying and increased fire hazard on a much shorter time scale than forests. Partners suggest time scales of weeks-to-months for rangeland and 2-5 years for forest drought input into the model. Furthermore, a more robust measure of vegetation growth and decline could be generated using NDVI anomaly. Comparing NDVI in the model year to the mean ten-year NDVI would indicate departures from typical biomass cycle, potentially highlighting problematic fuel dynamics and providing utility in the model.

The team hoped to conduct robust time series analysis, including cross-correlation analysis, to compare drought indicators EDDI and ESI to known proxies of plant vitality like NDVI and NDMI. This could potentially unlock clues as to forcing influence between drought and plant health, solidifying the utility of using drought indicators like EDDI and ESI in wildfire hazard modeling. While the team performed some analysis and visualization of time series data, periodicity complications and time limited the scope. Additionally, while the analog wildfire hazard model was most practical for ensuring completion during the first term and adoption by partners, a machine learning (ML) classification approach could produce improved results. Experimenting with variable importance and various ML classifiers, partitioning known fire pixels in a given year into testing and training data, and running these algorithms with existing drought, vegetation, landcover, and topography data as independent variables could generate highly effective and modern tools for partners to best prioritize limited fire mitigation resources.

Another area for future optimization could be the inclusion of ECOsystem Spaceborne Thermal Radiometer Experiment on Space Station (ECOSTRESS) data for ESI at 30m resolution, available from 7/9/2018 to present. It would be interesting to compare both drought indicator time series results and wildfire hazard model performance with those from SERVIR Global's 5km resolution ESI data, used in this study. Due to the planned retirement of the Terra and Aqua satellites which house the MODIS sensors, the incorporation of ET data from this newer data source would ensure long-term applicability and practicability of including ET-derived drought indicators in Idaho's state drought and wildfire mitigation protocols.

5. Conclusions

The team found that spikes in EDDI up to the 1.5 threshold occurred during the years with the most area burned- 2015 and 2021. Similar patterns did not take place during mesic, low-fire years. Furthermore, the team established that the difference between median growing season and fire season NDVI followed different distributions in high fire years and low fire years, suggesting that the phenomenon described by Li et al. (2020) for the Owyhee Basin in Southwestern Idaho could hold in other regions, including the study area. The team noticed that this effect predominantly occurred in rangeland, possibly due to forests' generally high NDVI levels and resilience in the face of short-scale drought pressures. This added to the importance of following through on the insight that forest and rangeland ought to be treated differently in the model. These landcovers could reveal greater insights treated separately, especially if considered over different time windows, though different drought indicators might also offer benefits.

The wildfire hazard model seemed to perform best during years with elevated fire occurrence and burned area, like 2015. The team took this as a sign that in general, the static, unchanging nature of many of the input variables established a baseline hazard score for each pixel across all models, limiting differentiation of fire hazard across years. The imperfect nature of the accuracy assessments performed on these models might also have contributed to the general increased performance in high fire years. Counting True Positives without adjustments for overprediction, meant that the highest accuracies were observed when the dependent, predicted variable of fire occurrence was at its highest. Finding alternative model construction schema or alternative variables that increase True Positives while maintaining or, ideally, decreasing False Positives should be a goal for the second term of the project. A ML classification approach may assist in creating a more dynamic and accurate model, taking into account all variables' weights on a yearly, rather than a static, basis.

Clear wet year/dry year performance differences and modest differences between EDDI models and ESI models emphasize the opportunity to improve accuracy and usefulness of the model. Leveraging differences in EDDI and ESI's underlying properties could help. EDDI, which assumes non-moisture limited conditions and provides potential ET for a system with sufficient water, is driven primarily by solar radiation, wind, humidity, and cloud cover. Because it does not account for real ET, it may offer better observation of hot, dry conditions when precipitation or other sources of water are limited, like in 2015 and 2021. ESI, on the other hand, estimates real ET based on actual moisture conditions. EDDI and ESI track together in non-moisture limited conditions; however, when moisture is limited, continued dry conditions will force EDDI to continue to rise even as real ET and ESI level off and begin to decline. The team hypothesized that these differences might have explained some discrepancies in accuracy for EDDI and ESI in wet and dry years.

Ultimately, modeling wildfire occurrence and hazard, and especially assessing accuracy of fire hazard models, remains elusive due in part to the probabilistic nature of fire – even the highest risk areas burn only when sporadic and unpredictable ignition sources present themselves. This likely contributed to increased accuracy when fire did occur, and certainly complicated efforts at quantifying model performance. The team finished the term excited to pass off this work to another motivated Idaho Wildfires team to further a practical, useful wildfire hazard product that partners can continue to use and improve.

6. Acknowledgments

The authors would like to thank our Fellow, Brandy Nisbet-Wilcox, Science Advisor, Keith Weber, and the ISU GIS TReC lab for their invaluable advice and access to excellent computing resources and datasets. The team also thanks DEVELOP Project Coordination Fellows Tamara Barbakova and Robert Cecil Byles for their guidance and editing.

Finally, a big thank you to the project partners Susan Cleverly, Mary Mott, & Lorrie Pahl (IOEM), David Hoekema (IDWR), and Tyre Holfeltz (IDL) for guiding the team's research toward maximum impact and scalability in hazard planning processes.

Any opinions, findings, and conclusions or recommendations expressed in this material are those of the author(s) and do not necessarily reflect the views of the National Aeronautics and Space Administration.

This material is based upon work supported by NASA through contract NNL16AA05C.

7. Glossary

Arid region – A distinct area that receives less than 10 inches of precipitation per year
Biomass – Renewable organic material that comes from plants and animals
E_0 – Evaporative demand; represents the potential ET in a non-surface moisture limited system
Earth observations – Satellites and sensors that collect information about the Earth's physical, chemical, and biological systems over space and time
Ecoregion – An ecologically and geographically defined area which contains characteristic, geographically distinct assemblages of natural communities and species
EDDI – Evaporative Demand Drought Index; indicates the anomaly of evaporative demand (E_0) summed over a specified time period and ranked in comparison to previous years before being incorporated into an inverse normal approximation.
ESI – Evaporative Stress Index; indicates the anomaly of ET composited over a specified time window
ET – evapotranspiration; the sum of evaporation from the land surface plus transpiration from plants
Landcover – The physical land type, e.g., forests, wetlands, impervious surfaces, agriculture, and other land and water types
Landsat – A series of Earth-observing satellite missions managed jointly by NASA and the U.S. Geological Survey

Mesic – Containing a moderate amount of moisture
MODIS – Moderate Resolution Imaging Spectroradiometer; An instrument aboard NASA's Terra and Aqua satellites
NDMI – Normalized Difference Moisture Index; A spectral vegetation index using near infrared and shortwave infrared wavelengths to estimate vegetation moisture
NDVI – Normalized Difference Vegetation Index; A spectral vegetation index using near infrared and red wavelengths to estimate vegetation photosynthetic activity.
WUI – Wildland Urban Interface is an area where developed lands interact with undeveloped lands and includes the infrastructure and natural resources communities rely on for existence.

8. References

Apurv, T., & Cai, X. (2021). Regional Drought Risk in the Contiguous United States. *Geophysical Research Letters*, *48*(5), e2020GL092200. https://doi.org/10.1029/2020GL092200

Brown, C. F., Brumby, S. P., Guzder-Williams, B., Birch, T., Hyde, S. B., Mazzariello, J., Czerwinski, W., Pasquarella, V. J., Haertel, R., Ilyushchenko, S., Schwehr, K., Weisse, M., Stolle, F., Hanson, C., Guinan, O., Moore, R., & Tait, A. M. (2022). Dynamic World, Near real-time global 10 m land use land cover mapping [Data Set]. *Scientific Data*, *9*(1), 251. https://doi.org/10.1038/s41597-022-01307-4

Chuvieco, E., Aguado, I., Yebra, M., Nieto, H., Salas, J., Martín, M. P., Vilar, L., Martínez, J., Martín, S., Ibarra, P., de la Riva, J., Baeza, J., Rodríguez, F., Molina, J. R., Herrera, M. A., & Zamora, R. (2010). Development of a framework for fire risk assessment using remote sensing and geographic information system technologies. *Ecological Modelling, 221*(1), 46–58. https://doi.org/10.1016/j.ecolmodel.2008.11.0177

Dennison, P. E., Brewer, S. C., Arnold, J. D., & Moritz, M. A. (2014). Large wildfire trends in the western United States, 1984–2011. *Geophysical Research Letters*, *41*(8), 2928–2933. https://doi.org/10.1002/2014GL059576

Du, J., & J. S. Kimball. (2021). *Daily Global Land Surface Parameters Derived from AMSR-E and AMSR2, Version 3, near-surface Vapor Pressure Deficit* [Data set]. Boulder, Colorado USA. NASA National Snow and Ice Data Center Distributed Active Archive Center. http://dx.doi.org/10.5067/JIKQZ6WO5C5M

LANDFIRE, Earth Resources Observation and Science Center (EROS) (2020). *LANDFIRE 2020 Existing Vegetation Type (EVT) CONUS LF 2020* [Data set]. https://www.landfire.gov [Accessed 7/11/2022].

Hanson, R. (1991). *Evapotranspiration and Droughts. U.S. Geological Survey. (No. 2375; National Water Summary 1988-89--Hydrologic Events and Floods and Droughts: U.S. Geological Survey Water-Supply Paper*, pp. 99–104) https://geochange.er.usgs.gov/sw/changes/natural/et/

Hobbins, M. T., Wood, A., McEvoy, D. J., Huntington, J. L., Morton, C., Anderson, M., & Hain, C. (2016). *Evaporative Demand Drought Index CONUS 1980–2022* [Data set]. NOAA Physical Sciences Laboratory. https://downloads.psl.noaa.gov/Projects/EDDI/CONUS_archive

Hobbins, M. T., Wood, A., McEvoy, D. J., Huntington, J. L., Morton, C., Anderson, M., & Hain, C. (2016). The Evaporative Demand Drought Index. Part I: Linking drought evolution to variations in evaporative demand. *Journal of Hydrometeorology*, *17*(6), 1745–1761. https://doi.org/10.1175/JHM-D-15-0121.1

Idaho Department of Lands (IDL) (2022). *Wildland Urban Interface (WUI)* [Unpublished dataset].

Landsat Missions (n.d.) *Landsat Normalized Difference Moisture Index*. [Data set]. U.S. Geological Survey. https://www.usgs.gov/landsat-missions/normalized-difference-moisture-index

Landsat Missions (n.d.) *Landsat Normalized Difference Vegetation Index*. [Data set]. U.S. Geological Survey. https://www.usgs.gov/landsat-missions/landsat-normalized-difference-vegetation-index

Landsat Missions (n.d.). *Using the USGS Landsat Level-1 Data Product.* [Data set]. U.S Geological Survey. https://www.usgs.gov/landsat-missions/using-usgs-landsat-level-1-data-product

Li, Z., Shi, H., Vogelmann, J. E., Hawbaker, T. J., & Peterson, B. (2020). Assessment of fire fuel load dynamics in shrubland ecosystems in the Western United States using MODIS products. *Remote Sensing*, *12*(12), 1911. https://doi.org/10.3390/rs12121911

Lozano, F. J., Suárez-Seoane, S., & de Luis, E. (2007). Assessment of several spectral indices derived from multi-temporal Landsat data for fire occurrence probability modelling. *Remote Sensing of Environment*, *107*(4), 533–544. https://doi.org/10.1016/j.rse.2006.10.001

Lukas, J., Hobbins, M., Imtiaz, R. (September, 2017). *The EDDI User Guide v1.0.* Physical Sciences Laboratory, NOAA. https://psl.noaa.gov/eddi/pdf/EDDI_UserGuide_v1.0.pdf

National Integrated Drought Information System (NIDIS) (2022). *Evaporative Stress Index (ESI).* https://www.drought.gov/data-maps-tools/evaporative-stress-index-esi

Riley, K. L., Abatzoglou, J. T., Grenfell, I. C., Klene, A. E., & Heinsch, F. A. (2013). The relationship of large fire occurrence with drought and fire danger indices in the western USA, 1984–2008: The role of temporal scale. *International Journal of Wildland Fire*, *22*(7), 894. https://doi.org/10.1071/WF12149

Scasta, J. D., Weir, J.M., & Stambaugh, M.C. (2016). Droughts and wildfires. *Rangelands*, *38*(4), 197–203. https://doi.org/10.1016/j.rala.2016.06.003

SERVIR Global Data Catalogue (2022). *Evaporative Stress Index (ESI).* [Data set]. SERVIR Global. https://gis1.servirglobal.net/geonetwork/srv/eng/catalog.search#/metadata/97082c3e-a136-4689-bcdf-517a4bb6907f

Sohrabi, M. M., Ryu, J. H., Abatzoglou, J., & Tracy, J. (2013). Climate extreme and its linkage to regional drought over Idaho, USA. *Natural Hazards*, *65*(1), 653–681. https://doi.org/10.1007/s11069-012-0384-1

U.S. Geological Survey (2022). *National Watershed Boundary Dataset (WBD) - USGS National Map* [Data set]. https://hydro.nationalmap.gov/arcgis/rest/services/wbd/MapServer [Accessed 6/30/2022]

U.S. Geological Survey (2021). *MOD13Q1 v006- MODIS/Terra Vegetation Indices 16-Day L3 Global 250m SIN Grid* [Data set]. https://lpdaac.usgs.gov/products/mod13q1v006/ [Accessed 6/30/2022].

U.S. Geological Survey (2021). *Path/row 042/028:042/027 (3/1/2013 - 9/30/2021), Landsat 8 Operational Land Imager and Thermal Infrared Sensor Collection 2 Level-1* [Data set]. https://earthexplorer.usgs.gov/ [Accessed 7/11/2022].

U.S. Geological Survey (n.d.) *What are the band designations for the Landsat Satellites? (FAQ).* USGS Mapping, Remote Sensing, and Geospatial Data. https://www.usgs.gov/faqs/what-are-band-designations-landsat-satellites

Weber, K. T., *Idaho State University GIS Training and Research Center (2022). Historic Fires Database (HFD)* v3.0 [Data set]. https://giscenter.isu.edu/research/Techpg/HFD/

Weber, K. T., Idaho State University GIS Training and Research Center (2016). *NASA RECOVER National Elevation Dataset (NED)* https://giscenter.rdc.isu.edu/portal/home/item.html?id=0224dcdef411482fbf82ea5de0f90d43

Weber, K. T., & Yadav, R. (2020). Spatiotemporal trends in wildfires across the Western United States (1950–2019). *Remote Sensing*, *12*(18), 2959. https://doi.org/10.3390/rs12182959

Yadav, R., Weber, K., Buffalo, K. (2020). *Investigating Effects of Weather and Climate on Biomass Production in the Intermountain West.* [Unpublished Manuscript]. https://giscenter.isu.edu/research/Techpg/NASA_ISGC/pdf/Yadav_Climate_Pilot.pdf

Yang, Y., Anderson, M. C., Gao, F., Wardlow, B., Hain, C. R., Otkin, J. A., Alfieri, J., Yang, Y., Sun, L., & Dulaney, W. (2018). Field-scale mapping of evaporative stress indicators of crop yield: An application over Mead, NE, USA. *Remote Sensing of Environment*, *210*, 387–402. https://doi.org/10.1016/j.rse.2018.02.020

9. Appendices

Appendix A

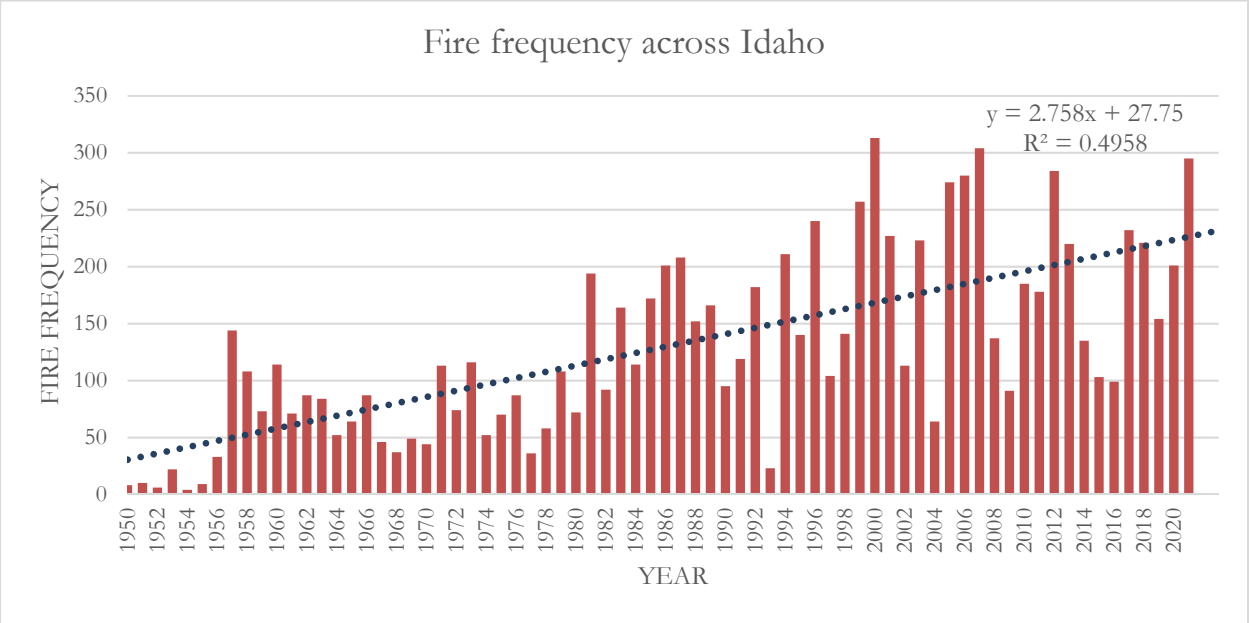

Figure A1. Linear regression of annual fire frequency across Idaho between 1950 and 2021 ($r^2 = 0.5$). It is likely more fires occurred than reported in the Historic Fires Database and that more data is missing from earlier study dates.

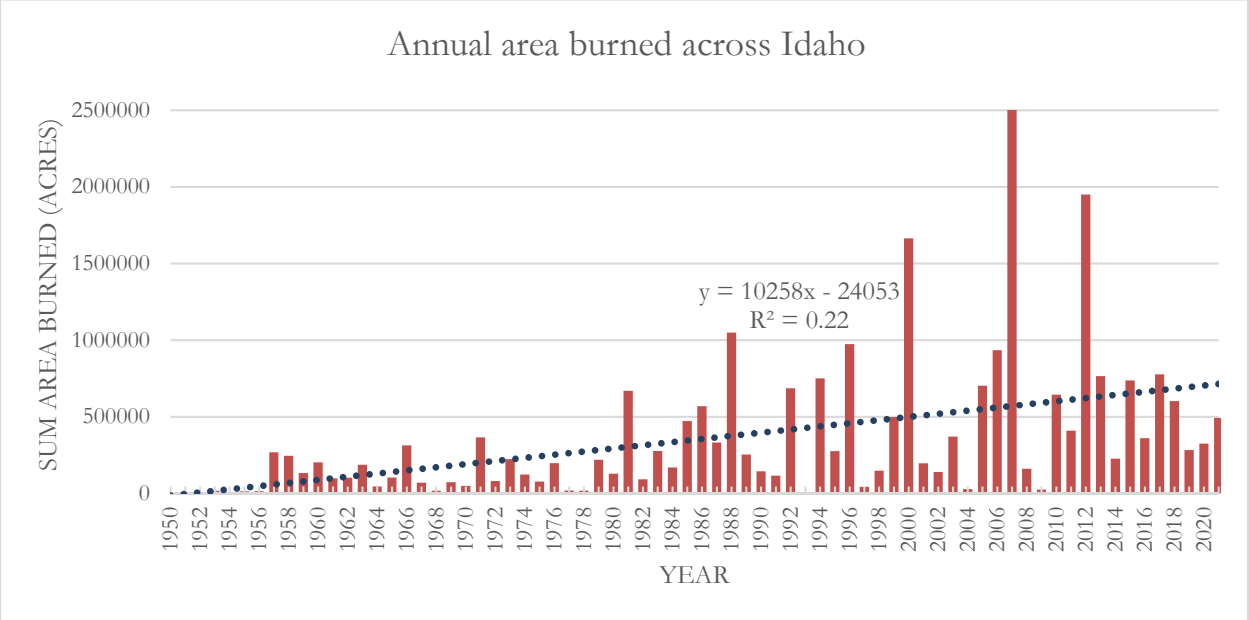

Figure A2. Linear regression of the annual total area burned across Idaho between 1950 and 2021 ($r^2 = 0.23$).

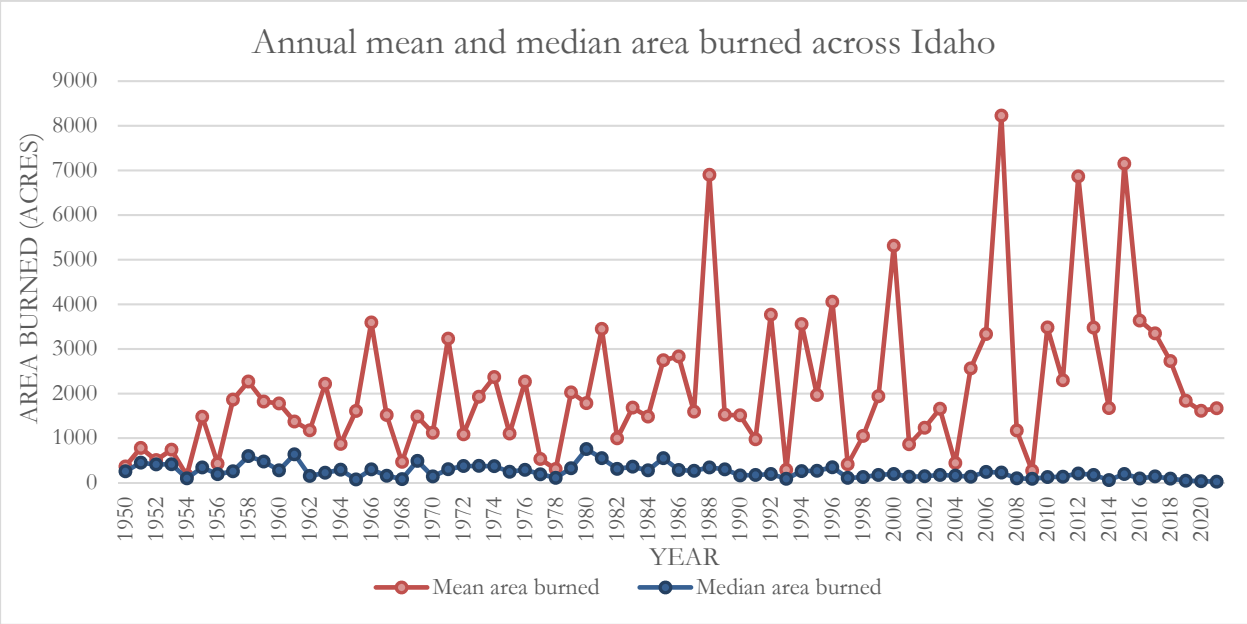

Figure A3. Annual mean and median area burned across Idaho from 1950 to 2021. The increasing disparity between the mean and median indicates higher incidence of mega fires in recent years.

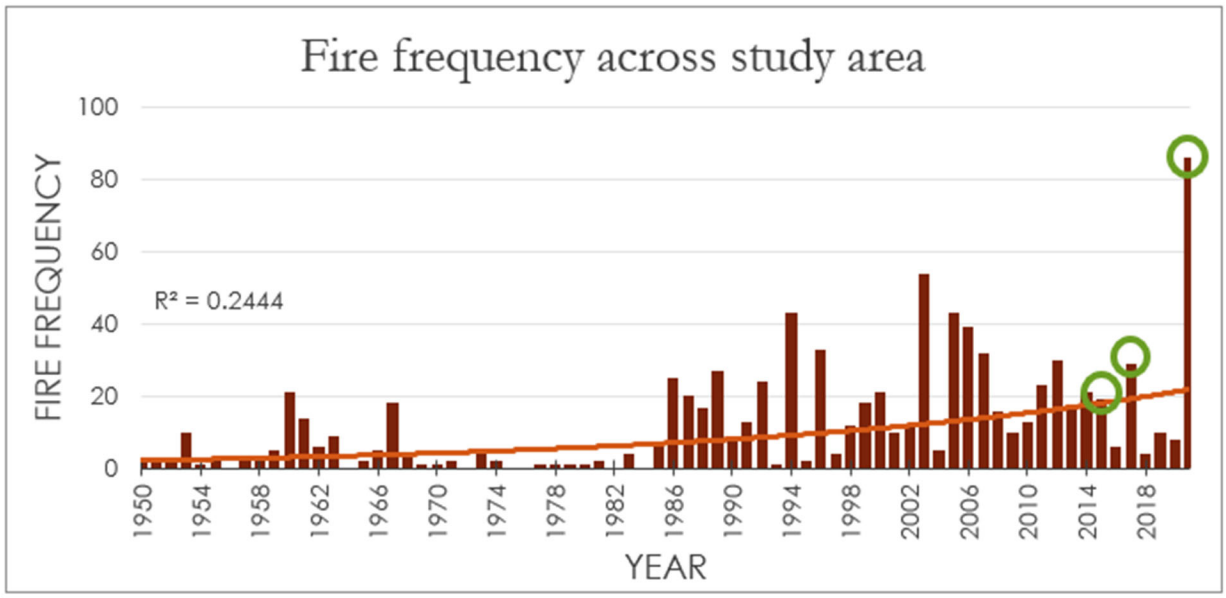

Figure A4. Annual fire frequency in the study area with key high-fire years 2015, 2017, 2021 highlighted with green circles.

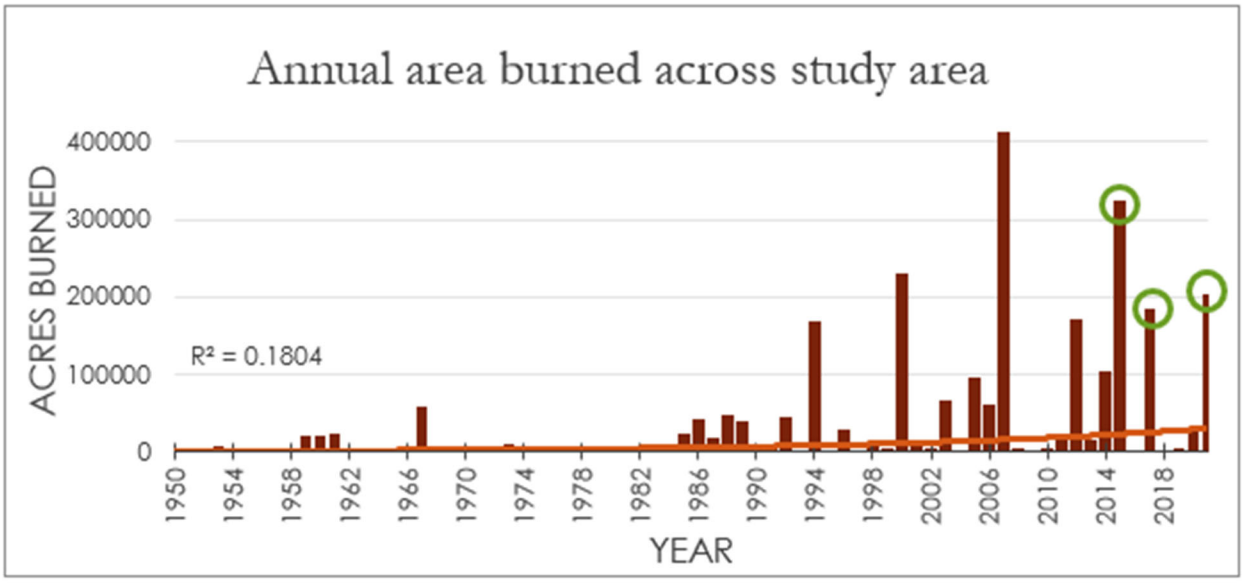

Figure A5. Annual burned area in the study area with key high-fire years 2015, 2017, 2021 highlighted with green circles.

Appendix B

$$NDVI = \frac{(NIR-Red)}{(NIR+Red)} \quad \text{(B1)}$$

Equation B1: Normalized Difference Vegetation Index (NDVI) equation. *NIR* refers to the Near Infrared band value (Band 5, 0.85-0.88 μm) and *Red* refers to the visible red band value (Band 4, 0.64-0.67 μm) of NASA's Landsat 8/9 OLI sensor. ("Normalized Difference Vegetation Index," n.d.; "What are the band designations for the Landsat Satellites?," n.d.)

$$NDMI = \frac{(NIR-SWIR)}{(NIR+SWIR)} \quad \text{(B2)}$$

Equation B2: Normalized Difference Moisture Index (NDMI) equation. *NIR* refers to the Near Infrared band value (Band 5, 0.85-0.88 μm) and *SWIR* refers to the Short-wave Infrared band (Band 6, 1.57-1.65 μm) of NASA's Landsat 8/9 OLI sensor. ("Normalized Difference Moisture Index," n.d.; "What are the band designations for the Landsat Satellites?," n.d.)

$$EDDI = W - \frac{C_0+C_1W+C_2W^2}{1+d_1W+d_2W^2+d_3W^3} \quad \text{(B3)}$$

$$W = \begin{cases} \sqrt{-2\ln[P(E_{0_i})]} & P(E_{0_i}) \le 0.5 \\ \sqrt{-2\ln[1-P(E_{0_i})]} & P(E_{0_i}) > 0.5 \end{cases} \quad \text{(a)}$$

$$P(E_{0_i}) = \frac{i-0.33}{n+0.33'} \quad \text{(b)}$$

Equations B3, B3a, B3b: Evaporative Demand Drought Index (EDDI) equation, including associated variables, reproduced from Hobbins et al., 2016. $P(E_{0i})$ indicates the probability of a given sum of E_0 over a given time period, i indicates the rank of E_0 over the time series, and n is the period in years. EDDI is then calculated from the inverse normal approximation with following constants: C_0 = 2.515517; C_1 = 0.802853, C_2 = 0.010328; d_1 = 1.432788; d_2 = 0.189269; d_3 = 0.001308 (Hobbins et al., 2016).

$$ESI$$

$$f_{RET} = \frac{ETd}{ETod} \quad \text{(B4)}$$

$$v(d,y_k,i,j)' = \frac{\langle v(d,y_k,i,j)\rangle - \frac{1}{n}\sum_{k=1}^{k=n}\langle v(d,y_k,i,j)\rangle}{\sigma(d,i,j)} \quad \text{(a)}$$

Equation B4, B4a: Evaporative Stress Index (ESI) values represent standardized anomalies (computed as in (a)) in f_{RET}, normalized by reference ET. f_{RET} simply represents relative ET (the actual-to-reference ET ratio: ETd is the actual daily ET and $ETod$ refers to the hourly reference, time-integrated ET to a daily value). In (a), $\langle v(d,y_k,i,j)\rangle$ is the f_{RET} composite for day d, year y, and i,j grid location, $v(d,y,i,j)$ is the value on day d, n is the number of years in the period of record, and $\sigma(d,i,j)$ is the standard deviation in v for that compositing interval- essentially turning f_{RET} into a z-score. (Yang et al., 2018).

Appendix C

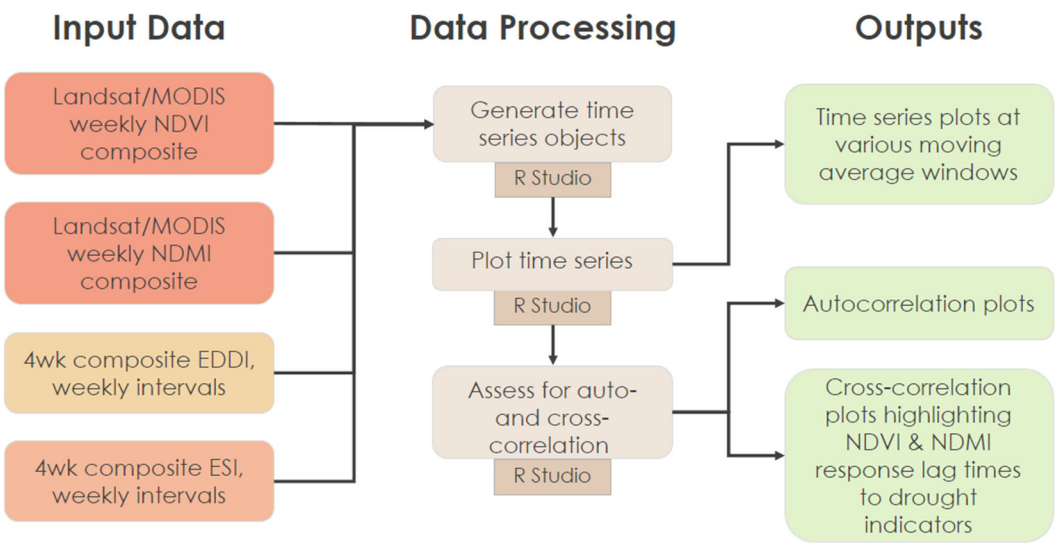

Figure C1. Flowchart of Drought Indicator Analysis performed during Term 1 of Idaho Wildfires.

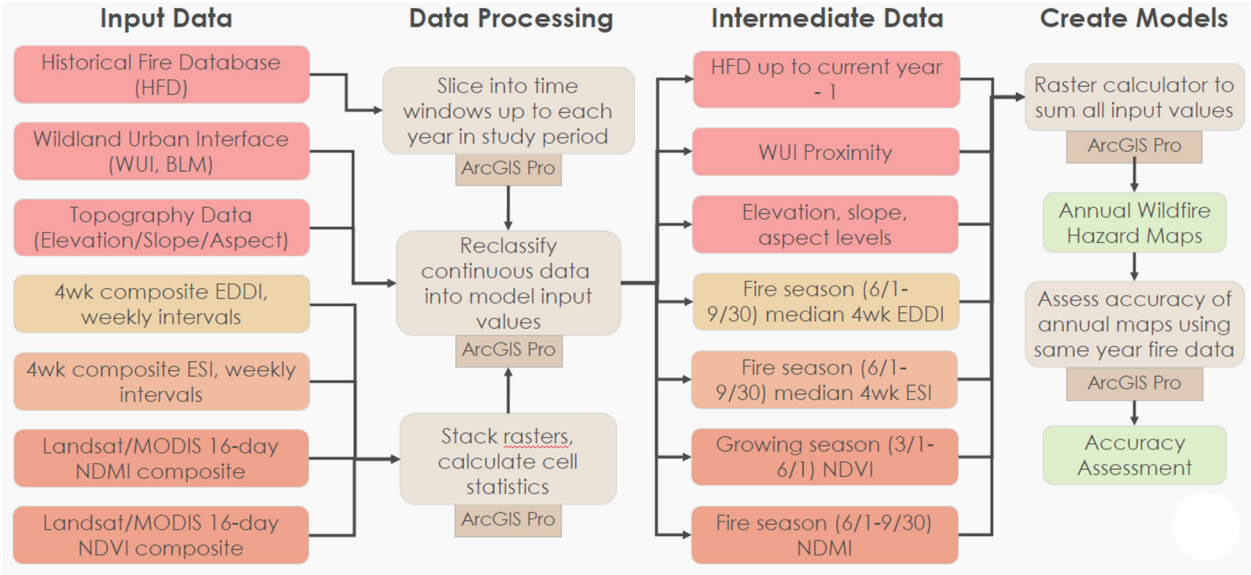

Figure C2: Flowchart of Wildfire Hazard Modeling performed during Term 1 of Idaho Wildfires.

Appendix D

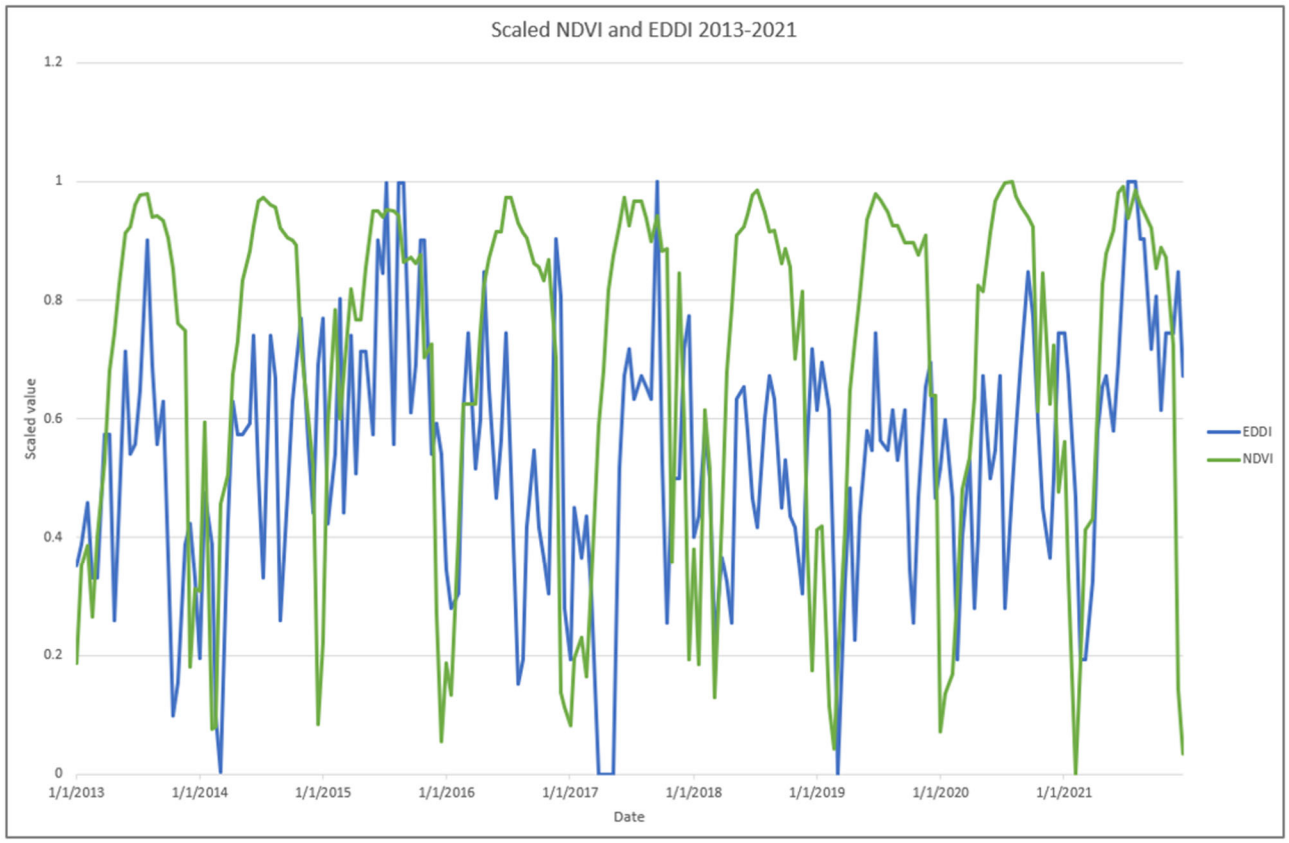

Figure D1: Time series plot of median NDVI (green) and median EDDI (blue) over the study period (2013-2021). Both variables have been scaled to a range of 0-1 for ease of comparison.

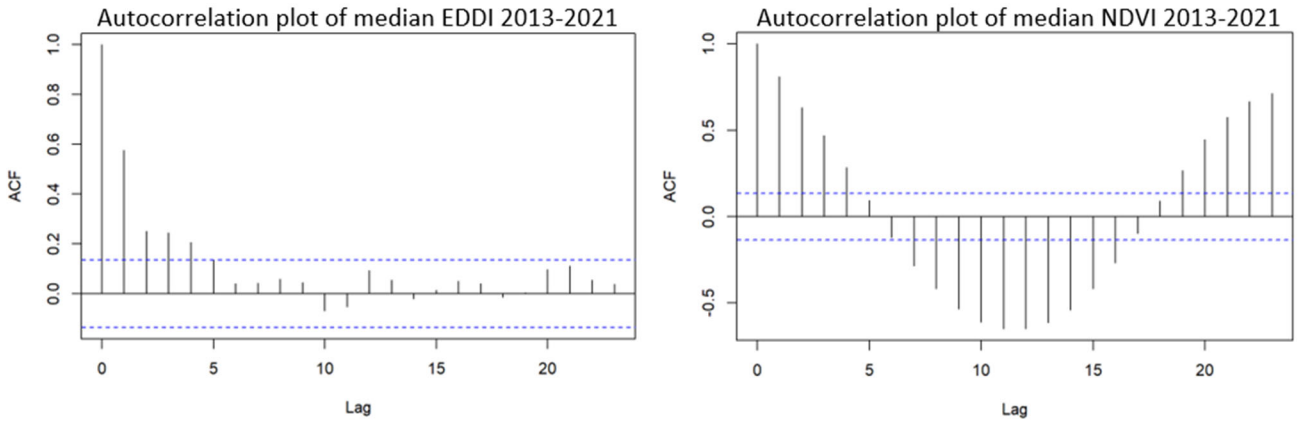

Figure D2: Autocorrelation plots from R Studio showing 2013-2021 median EDDI and NDVI autocorrelation. Lag time units of 2 weeks (each lag unit of 1 is a 2 week period). ACF indicates correlation of the dataset with itself at the indicated lag time. Horizontal dashed blue lines indicate the 95% confidence interval for correlation. Notice clear autocorrelation in NDVI over the study period – this prevented adequate cross-correlation analysis between median EDDI and median NDVI.

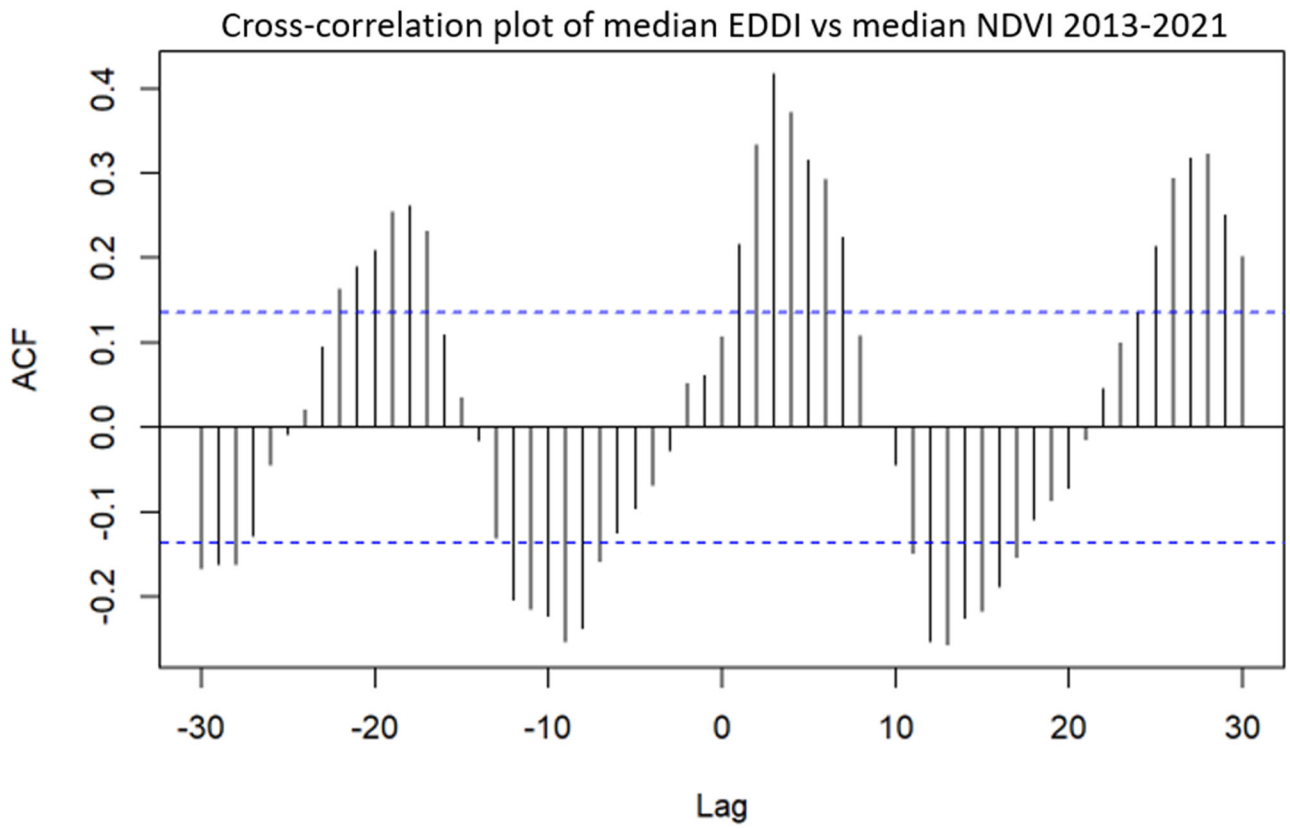

Figure D3: Cross-correlation plot from R Studio showing 2013-2021 median EDDI and NDVI. Lag time units of 2 weeks (each lag unit of 1 is a 2-week period). ACF indicates correlation of the EDDI at a given lag time with NDVI at time 0. Horizontal dashed blue lines indicate the 95% confidence interval for correlation. Due to autocorrelated nature of NDVI data, this cross-correlation is flawed and was not able to be used by the team.